RSC Advances

PAPER

View Article Online
View Journal | View Issue

Cite this: *RSC Adv.*, 2026, **16**, 8037

Enhanced NH_3 uptake and selectivity at low pressure in monolithic MOF-808 metal–organic gels incorporating $CuCl_2$

Chuan Zhou,†[a] Feng Liu,†[a] Chao Zheng,[a] Qiong Wu,[a] Hantong Chen,[a] Liangyu Li,[b] Jiayu Zhai,[a] Li Li,*[a] Bo Yang*[a] and Pingwei Ye *[a]

Received 10th October 2025
Accepted 7th January 2026

DOI: 10.1039/d5ra07740k

rsc.li/rsc-advances

The capture and separation of trace NH_3 from industrial processes or polluted air remains a significant challenge. Herein, we report a monolithic $CuCl_2$@G808 metal–organic gel achieving an NH_3 uptake of 2.23 mmol g^{-1} at 298 K and 0.002 bar: a 79% enhancement compared to pristine G808. The ideal adsorbed solution theory (IAST) selectivity reaches 2.8 × 10^3 for NH_3/N_2 and 4.9 × 10^5 for NH_3/H_2 at 298 K, ranking among the highest reported values. *In situ* FTIR and XPS analyses reveal that the excellent performance mainly originates from two synergistic mechanisms: (i) coordination between NH_3 and Cu^{2+} sites, and (ii) hydrogen bonding between NH_3 and Cl^- sites.

Introduction

Ammonia (NH_3) is an important chemical feedstock, mainly produced by the Haber–Bosch process, and widely used in refrigeration, energy, and fertilizer industries.[1,2] At the same time, ammonia is a highly toxic and corrosive gas, mostly derived from the inadvertent or intentional emission, which causes severe damage to human health and the environment even at low concentrations.[3] Therefore, efficient capture and separation of trace NH_3 from the NH_3 production process or polluted air is of great significance for improving NH_3 production efficiency and reducing energy consumption, and alleviating impacts on the environment and human health.

Metal–organic frameworks (MOFs) adopt structural designability and diversity, abundant active sites, and high porosity, enabling them prospective candidates for real-world NH_3 capture and separation. Several representative MOFs such as LiCl@MIL-53-$(OH)_2$-43.4,[4] LiCl@G66-OH-35.7,[5] IL@MIL-101(Cr),[6] Mg_2(dobpdc),[7] Ni_acryl_TMA,[8] Cu_2Cl_2BBTA,[9] MOF-303(Al),[10] MOF-253(Al)-$NiCl_2$-2,[11] MFU-4,[12] Cu(cyhdc),[13] $Co(NA)_2$,[14] MFM-300(V^{IV}),[15] Cu(BDC),[16] UiO-66-Cu^{II},[17] DUT-6-$(OH)_2$,[18] [Mn_2Cl_2BTDD],[19] Fe-soc-MOF,[20] and MFM-300(Sc)[21] have demonstrated outstanding NH_3 capture performance even at low pressure. However, their connatural limitations such as low NH_3 adsorption capacity and separation ability at extremely low pressure, high production cost, limited stability, and powder state problem preclude their potential application for NH_3 efficient capture and separation. Therefore, there is an urgent need to fabricate granular high-performance MOFs adsorbents possessing remarkable NH_3 adsorption and separation ability at ultra-low pressure and facile preparation process.

Metal–organic framework gels (MOGs), as a novel self-shaping material, have come to prominent attention owing to its adjustable aperture from micropore to mesopore/macropore, high adsorptive capacity, and easy large-scale preparation.[22] MOGs can be facilely fabricated by regulating reaction conditions such as metal source, reactant concentration, solvent, and temperature.[23,24] Up to now, MOGs have demonstrated excellent capture performance in many fields such as methane storage,[25,26] CO_2 capture and storage,[27,28] volatile organic compounds capture,[29–31] water remediation,[32,33] chemical warfare agents decontamination,[34,35] toxic chemical filtration.[36–38] However, there are few reports on the efficient capture and separation of NH_3 using MOGs, especially under ultra-low pressure.

$CuCl_2$ possesses an exceptional NH_3 uptake, but its application is greatly limited due to its powder state. Based on the above advantages of MOGs, herein, MOF-808 metal–organic framework gel (labeled as G808) is chosen as the platform due to its excellent stability to NH_3. Thus, $CuCl_2$@G808 composite is prepared in water by a facile impregnation strategy at 80 °C. $CuCl_2$@G808 containing 2.55 wt% of $CuCl_2$ shows excellent low-pressure NH_3 uptake (2.23 mmol g^{-1}) at 298 K and 0.002 bar, which displays enhancement of 79% than that of the pristine G808. Notable, highly selective adsorption of trace NH_3 was also obtained at 298 K. Furthermore, molecular-level insights into the adsorption mechanism were elucidated through combined spectroscopic analyses.

[a]*State Key Laboratory of Chemistry for NBC Hazards Protection, Beijing 102205, PR China. E-mail: lily97@buaa.edu.cn; dahema2007goodluck@163.com; yepw2001@163.com*

[b]*Yichang Office of the Army Equipment Department, Yichang 44300, PR China*

† These authors contributed equally to this work.

Result and discussion

Structure and morphology of $CuCl_2$@G808-X composites

G808 is firstly synthesized according to our previous work.[39] Then, $CuCl_2$@G808 composite is obtained by a facile impregnation strategy in water solution containing $CuCl_2$ at 80 °C for 24 h. The content of $CuCl_2$ loaded on G808 is 2.55% measured by ICP-OES. As observed in Fig. 1a, the PXRD pattern of G808 matches well with the simulated MOF-808 (CCDC: 1002672), as evidenced by the characteristic peaks at $2\theta = 4.4°$ and 8.6°.[40] Furthermore, the crystallinity of $CuCl_2$@G808 decreases compared with that of G808, suggesting that the crystal structure of the composite collapses after loading $CuCl_2$. SEM results also further confirm this conclusion (Fig. S1). In addition, no significant additional peaks are observed in the PXRD of the composite, indicating that $CuCl_2$ is evenly anchored in the nanopores of G808. Meanwhile, the uniform distribution of Cu and Cl elements in $CuCl_2$@G808 is verified by energy-dispersive X-ray spectroscopy (Fig. S2). Fig. 1b illustrates the TGA profiles of the samples. The initial mass reduction (303–373 K) is due to residual solvent volatilization, followed by two distinct degradation stages: framework collapse at 473–673 K and organic ligand decomposition at 673–1073 K.[40] Compared with G808, the thermal stability of $CuCl_2$@G808 slightly decreases from 743 K to 703 K, indicating that the introduction of $CuCl_2$ has a certain influence on the thermal stability of the composite. This result is in coincidence with that of XRD. Comparative FT-IR analyses reveal negligible spectral differences between pristine G808 and $CuCl_2$@G808 (Fig. 1c). Compared with G808, the peak of $CuCl_2$@G808 stemmed from the carboxylate ($-COO^-$) group undergoes some degrees of red shift from 1572 cm^{-1} to 1562 cm^{-1}, possibly through partial charge transfer from $-COO^-$ groups to Cu^{2+}.[41] Like G808, the $CuCl_2$@G808 composite also display characteristic IV isotherms for N_2 adsorption (Fig. 1d), indicating the existence of microporous and mesoporous features. This result is also validated by the pore size distribution (Fig. S3 and S4). Compared to G808, pore volume, surface area, and pore width of $CuCl_2$@G808 composite dramatically decrease due to the occupation of the pore space by $CuCl_2$ (Table S1).

NH_3 capture and separation

To study capture performance, NH_3 adsorption isotherms (Fig. 2) of G808 and $CuCl_2$@G808 composite are collected at 298 K and 1 bar. The isotherms show obvious hysteresis loops, suggesting the existing of strong interaction between NH_3 and active sites. Compared with G808 (9.6 mmol g^{-1}), the NH_3 capture capacity of the $CuCl_2$@G808 (8.1 mmol g^{-1}) slightly decreases due to the decrease of porosity at 298 K and 1 bar. However, the $CuCl_2$@G808 manifests a significantly enhanced uptake at low pressure. For example, the NH_3 adsorption capacity of $CuCl_2$@G808 can reach approximately 5.44 mmol g^{-1} at 0.1 bar, 3.65 mmol g^{-1} at 0.01 bar, and 2.23 mmol g^{-1} even at 0.002 bar (Fig. 2a), Compared to pristine G808, these

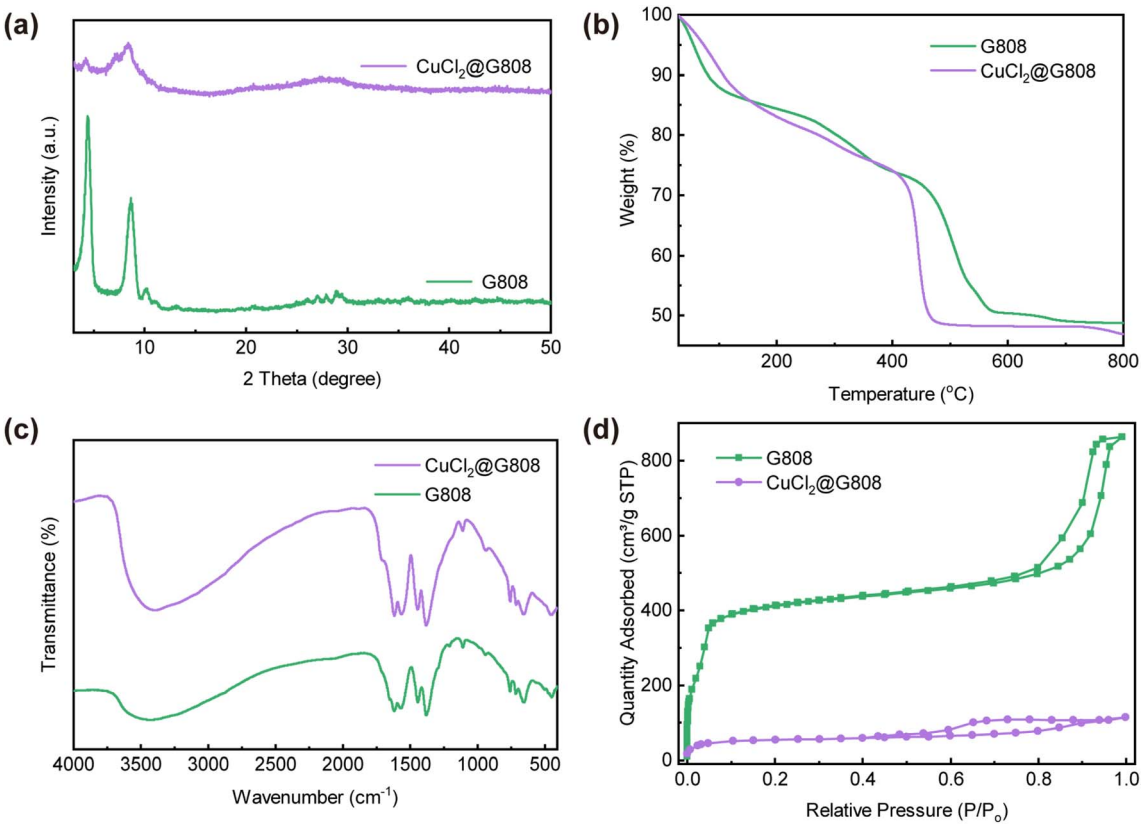

Fig. 1 (a) PXRD patterns, (b) TGA curves, (c) FT-IR spectra, and (d) N_2 adsorption–desorption isotherms of $CuCl_2$@G808.

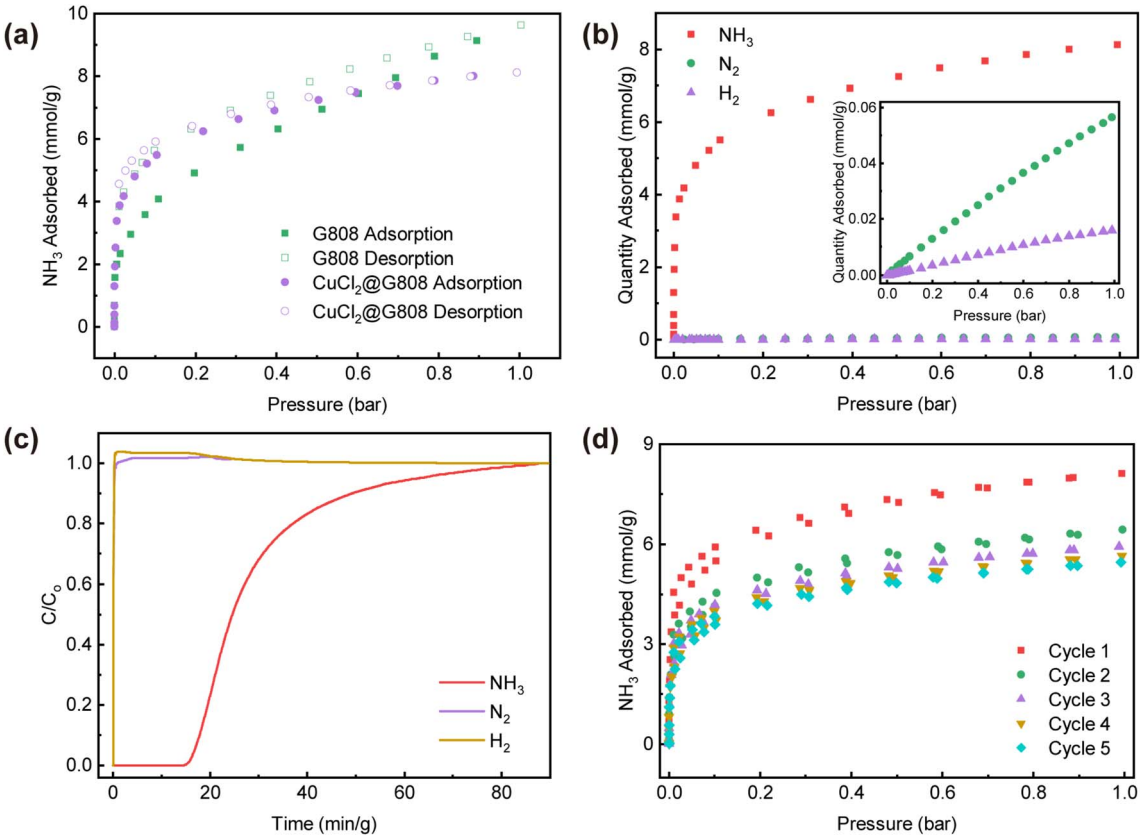

Fig. 2 (a) Adsorption–desorption isotherms of NH_3, (b) adsorption isotherms of $CuCl_2$@G808 for NH_3, N_2, and H_2, (c) breakthrough curves of $CuCl_2$@G808 for $NH_3/N_2/H_2$ mixtures, (d) NH_3 adsorption–desorption isotherms for different cycles of $CuCl_2$@G808 at 298 K.

values represent enhancement of 37%, 74%, and 79%, respectively. These results are comparable to the best-behaving values reported recently (Table S2), and indicate that our composite is conducive to the capture of low concentration NH_3. To validate this, N_2 and H_2 isotherms of $CuCl_2$@G808 are measured at 273 K and 298 K (Fig. 2b, S5 and S6). Notably, the adsorption capacities of N_2 (0.056 mmol g^{-1}) and H_2 (0.016 mmol g^{-1}) on $CuCl_2$@G808 at 298 K and 1 bar are significantly lower than that of NH_3 (8.1 mmol g^{-1}). This may be attributed to their weak affinity with the composite originated from low Q_{st} values (Fig. S7 and S8). The IAST-predicted selectivity values of $CuCl_2$@G808 reach 2.8×10^3 for NH_3/N_2 and 4.9×10^5 for NH_3/H_2 at 298 K, respectively (Fig. S9 and 10), surpassing most reported MOFs.[11,42] Furthermore, granular $CuCl_2$@G808 exhibits excellent self-shaping ability, facile synthesis, and low production cost, demonstrating its competitive and practical potential in low concentration NH_3 capture and separation.

Considering the valuable NH_3 industry synthesis, breakthrough experiments are adopted to validate the practical separation capability of $CuCl_2$@G808 for NH_3 using actual $NH_3/N_2/H_2$ mixtures (3% NH_3 in 25% N_2 and 72% H_2) (Fig. 2c). It is clearly observed that N_2 and H_2 are immediately escaped because of their low adsorption capacity, followed by NH_3 after 16.8 min g^{-1} accompanied by uptake of 3.9 mmol g^{-1}. Thus, $CuCl_2$@G808 can be considered as a superior adsorbent for selective separation of $NH_3/N_2/H_2$ at low NH_3 concentration. Five recycling experiment of $CuCl_2$@G808 is also carried out to study its practical performance (Fig. 2d and S11). NH_3 adsorption capacity of $CuCl_2$@G808 can be only maintained up to 5.4 mmol g^{-1} (67.1%) after five cycles at 298 K and 1 bar due to its partial structural collapse (Fig. S12 and S13). Meanwhile, about 50.7% of NH_3 is difficult to desorb due to the strong interaction between NH_3 and $CuCl_2$@G808.

Mechanism of NH_3 adsorption

To elucidate adsorption mechanism between $CuCl_2$@G808 and NH_3, a combination of spectroscopic techniques-including *in situ* FTIR and XPS spectra are employed (Fig. S14). After adsorption of NH_3, a new IR peak attributed to N–H deformation vibration emerges at 685 cm^{-1} (Fig. 3a), suggesting potential coordination between NH_3 and Cu^{2+}.[43] Besides, the C=O stretching vibration peak shifts from 1566 cm^{-1} to 1574 cm^{-1} (Fig. 3a) and the weak phenyl C–H peak at 3088 cm^{-1} disappear (Fig. 3b) after NH_3 adsorption, possibly due to hydrogen bonding between NH_3 and these groups.

The XPS survey spectrum of $CuCl_2$@G808 over the range of 0–1300 eV is presented in Fig. S15. Characteristic peaks corresponding to C 1s, O 1s, Zr 3d, Cu 2p, and Cl 2p are clearly observed, confirming the presence of these elements in the composite. Furthermore, XPS spectrum of $CuCl_2$@G808 after NH_3 adsorption is also recorded (Fig. 4). Following NH_3

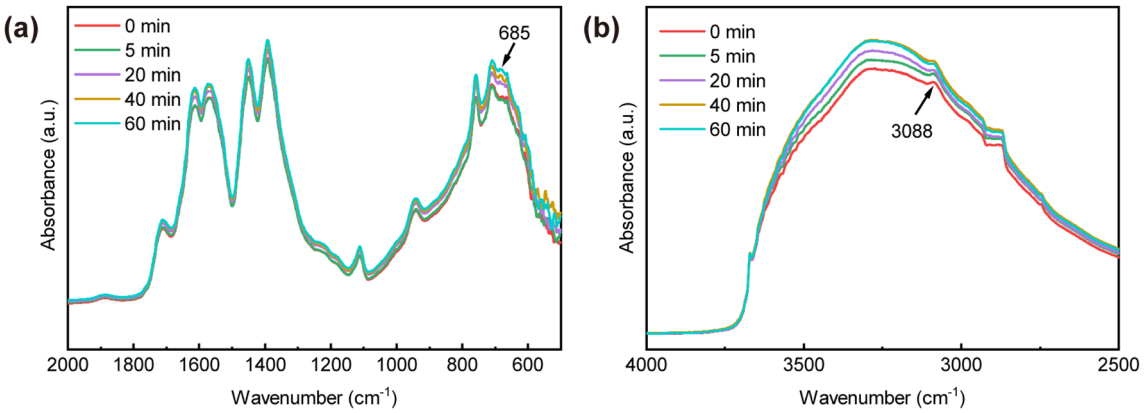

Fig. 3 (a) and (b) *In situ* FTIR spectra of $CuCl_2$@G808 during NH_3 uptake.

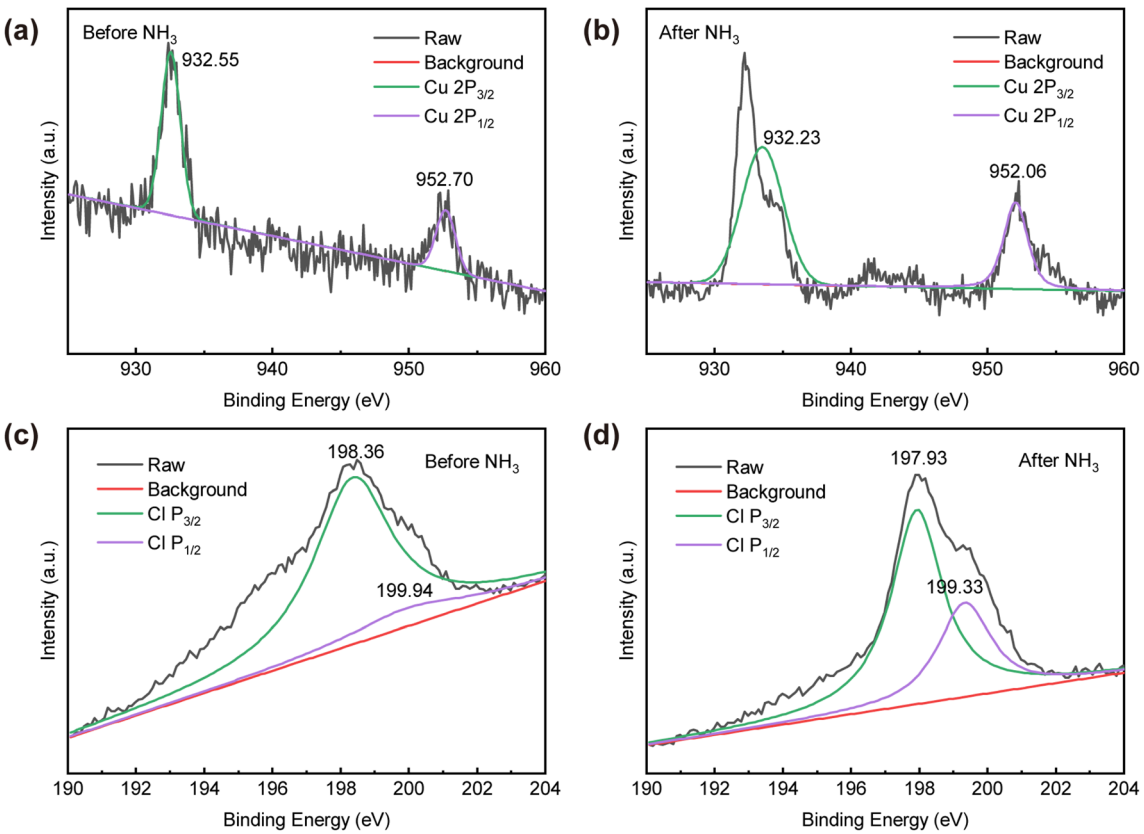

Fig. 4 XPS spectra of Cu 2p (a) and (b) and Cl 2p (c) and (d) for $CuCl_2$@G808 before and after NH_3 adsorption.

adsorption, the binding energies of Cu $2p_{3/2}$ and Cu $2p_{1/2}$ shift from 932.55 eV and 952.70 eV to 932.23 eV and 952.06 eV, respectively (Fig. 4a and b). This negative shift suggests enhanced electron density around Cu^{2+} due to coordination with the N atom of NH_3, consistent with electron donation from the adsorbate to the metal center.[43] Meanwhile, the Cl 2p peaks of $CuCl_2$@G808 at 199.94 eV and 198.36 eV decrease to 199.33 eV and 197.93 eV, respectively (Fig. 4c and d), attributed to hydrogen bonding between NH_3 and Cl^- sites.[4,43] These findings further validate that $CuCl_2$ incorporation enhances the NH_3 adsorption capacity of the composite at low pressure.

Conclusion

In summary, we develop a granular $CuCl_2$@G808 metal–organic gel *via* a simple aqueous-phase impregnation method. It is interesting to observe that $CuCl_2$@G808 demonstrates an exceptional NH_3 uptake (2.23 mmol g^{-1}) at 298 K and 0.002 bar, which exhibits 79% enhancement over pristine G808 and maintains 67.1% adsorption capacity after five adsorption–desorption cycles. On the other hand, $CuCl_2$@G808 achieves outstanding IAST selectivity for NH_3/N_2 (2.8×10^3) and NH_3/H_2 (4.9×10^5). *In situ* FTIR and XPS spectra reveal that low NH_3

pressure can be mainly explained by NH_3–Cu^{2+} coordination and hydrogen-bond networks. These findings advance the rational design of robust adsorbents for capturing and separating trace NH_3.

Conflicts of interest

The authors declare no conflict of interest.

Data availability

The authors declare that the data supporting the findings of this study are available within the paper and its supplementary information (SI) files. Should any raw data files be needed in another format they are available from the corresponding author upon reasonable request. Supplementary information is available. See DOI: https://doi.org/10.1039/d5ra07740k.

Acknowledgements

The Shiyanjia Lab (https://www.shiyanjia.com/) and Beishide Instrument technology (Beijing) Co., Ltd is gratefully thanked for providing instrumental facilities. C. Z. thanks National Natural Science Foundation of China Program (no. 22075319 and no. 22472200) for funding.

References

1 X. Tian, J. Qiu, Z. Wang, Y. Chen, Z. Li, H. Wang, Y. Zhao and J. Wang, *Chem. Commun.*, 2022, **58**, 1151–1154.
2 F. H. Nowrin and M. Malmali, *ACS Sustainable Chem. Eng.*, 2022, **10**, 12319–12328.
3 Y. Chen, Y. Wang, C. Yang, S. Wang, J. Yang and J. Li, *ACS Sustainable Chem. Eng.*, 2017, **5**, 5082–5089.
4 Y. Shi, Z. Wang, Z. Li, H. Wang, D. Xiong, J. Qiu, X. Tian, G. Feng and J. Wang, *Angew. Chem., Int. Ed.*, 2022, **61**, e202212032.
5 C. Zhou, J. Sun, C. Zheng, C.-A. Tao, L. Li, S. Bai, G. Fu, X. Yang, S. Zhang and S. He, *Sep. Purif. Technol.*, 2025, **374**, 133720–133726.
6 G. Han, C. Liu, Q. Yang, D. Liu and C. Zhong, *Chem. Eng. J.*, 2020, **401**, 126106–126112.
7 D. W. Kim, D. W. Kang, M. Kang, J.-H. Lee, J. H. Choe, Y. S. Chae, D. S. Choi, H. Yun and C. S. Hong, *Angew. Chem., Int. Ed.*, 2020, **59**, 22531–22536.
8 D. W. Kim, D. W. Kang, M. Kang, D. S. Choi, H. Yun, S. Y. Kim, S. M. Lee, J.-H. Lee and C. S. Hong, *J. Am. Chem. Soc.*, 2022, **144**, 9672–9683.
9 A. J. Rieth and M. Dincă, *J. Am. Chem. Soc.*, 2018, **140**, 3461–3466.
10 Z. Wang, Z. Li, X.-G. Zhang, Q. Xia, H. Wang, C. Wang, Y. Wang, H. He, Y. Zhao and J. Wang, *ACS Appl. Mater. Interfaces*, 2021, **13**, 56025–56034.
11 Y. Wang, Y. Shi, D. Xiong, Z. Li, H. Wang, X. Xuan and J. Wang, *Chem. Eng. J.*, 2023, **474**, 145307–145316.
12 R. Cao, Z. Chen, Y. Chen, K. B. Idrees, S. L. Hanna, X. Wang, T. A. Goetjen, Q. Sun, T. Islamoglu and O. K. Farha, *ACS Appl. Mater. Interfaces*, 2020, **12**, 47747–47753.
13 B. E. R. Snyder, A. B. Turkiewicz, H. Furukawa, M. V. Paley, E. O. Velasquez, M. N. Dods and J. R. Long, *Nature*, 2023, **613**, 287–291.
14 Y. Chen, B. Shan, C. Yang, J. Yang, J. Li and B. Mu, *J. Mater. Chem. A*, 2018, **6**, 9922–9929.
15 X. Han, W. Lu, Y. Chen, I. da Silva, J. Li, L. Lin, W. Li, A. M. Sheveleva, H. G. W. Godfrey, Z. Lu, *et al.*, *J. Am. Chem. Soc.*, 2021, **143**, 3153–3161.
16 Y. Chen, Y. Du, P. Liu, J. Yang, L. Li and J. Li, *Environ. Sci. Technol.*, 2020, **54**, 3636–3642.
17 Y. Ma, W. Lu, X. Han, Y. Chen, I. da Silva, D. Lee, A. M. Sheveleva, Z. Wang, J. Li, W. Li, *et al.*, *J. Am. Chem. Soc.*, 2022, **144**, 8624–8632.
18 I. Spanopoulos, P. Xydias, C. D. Malliakas and P. N. Trikalitis, *Inorg. Chem.*, 2013, **52**, 855–862.
19 A. J. Rieth, Y. Tulchinsky and M. Dinca, *J. Am. Chem. Soc.*, 2016, **138**, 9401–9404.
20 Z. Chen, X. Wang, R. Cao, K. B. Idrees, X. Liu, M. C. Wasson and O. K. Farha, *ACS Mater. Lett.*, 2020, **2**, 1129–1134.
21 P. Lyu, A. M. Wright, A. Lopez-Olvera, P. G. M. Mileo, J. Antonio Zarate, E. Martinez-Ahumada, V. Martis, D. R. Williams, M. Dinca, I. A. Ibarra, *et al.*, *Chem. Mater.*, 2021, **33**, 6186–6192.
22 B. M. Connolly, D. G. Madden, A. E. H. Wheatley and D. Fairen-Jimenez, *J. Am. Chem. Soc.*, 2020, **142**, 8541–8549.
23 J. Hou, A. F. Sapnik and T. D. Bennett, *Chem. Sci.*, 2020, **11**, 310–323.
24 B. Bueken, N. Van Velthoven, T. Willhammar, T. Stassin, I. Stassen, D. A. Keen, G. V. Baron, J. F. M. Denayer, R. Ameloot, S. Bals, *et al.*, *Chem. Sci.*, 2017, **8**, 3939–3948.
25 T. Tian, Z. Zeng, D. Vulpe, M. E. Casco, G. Divitini, P. A. Midgley, J. Silvestre-Albero, J.-C. Tan, P. Z. Moghadam and D. Fairen-Jimenez, *Nat. Mater.*, 2018, **17**, 174–180.
26 B. M. Connolly, M. Aragones-Anglada, J. Gandara-Loe, N. A. Danaf, D. C. Lamb, J. P. Mehta, D. Vulpe, S. Wuttke, J. Silvestre-Albero, P. Z. Moghadam, *et al.*, *Nat. Commun.*, 2019, **10**, 2345–2355.
27 C. Zhou, H. Li, H. Qin, B. Yuan, M. Zhang, L. Wang, B. Yang, C.-A. Tao and S. Zhang, *Chem. Eng. J.*, 2023, **467**, 143394–143402.
28 L. Li, S. Xiang, S. Cao, J. Zhang, G. Ouyang, L. Chen and C.-Y. Su, *Nat. Commun.*, 2013, **4**, 1774–1782.
29 H. Qin, J. Sun, X. Yang, H. Li, X. Li, R. Wang, S. He and C. Zhou, *J. Colloid Interface Sci.*, 2024, **655**, 23–31.
30 X. Zheng, H. Zhang, S. Rehman and P. Zhang, *J. Hazard. Mater.*, 2021, **411**, 125057–125067.
31 Z. Xianming, Z. Wu, J. Yang, S. Rehman and R. Cao, *ACS Appl. Mater. Interfaces*, 2021, **13**, 17543–17553.
32 W. Cui, X. Kang, X. Zhang and X. Cui, *J. Phys. Chem. Solids*, 2019, **134**, 165–175.
33 L. Luo, H. Huang, Y. Heng, R. Shi, W. Wang, B. Yang and C. Zhong, *J. Colloid Interface Sci.*, 2022, **628**, 705–716.
34 C. Zhou, B. Yuan, S. Zhang, G. Yang, L. Lu, H. Li and C.-A. Tao, *ACS Appl. Mater. Interfaces*, 2022, **14**, 23383–23391.

35 C. Zhou, L. Li, H. Qin, Q. Wu, L. Wang, C. Lin, B. Yang, C.-A. Tao and S. Zhang, *ACS Appl. Mater. Interfaces*, 2023, **15**, 54582–54589.
36 X. Wang, R. Su, Y. Zhao, W. Guo, S. Gao, K. Li, G. Liang, Z. Luan, L. Li, H. Xi, *et al.*, *ACS Appl. Mater. Interfaces*, 2021, **13**, 58848–58861.
37 X. Wang, L. Li, K. Li, R. Su, Y. Zhao, S. Gao, W. Guo, Z. Luan, G. Liang, H. Xi, *et al.*, *J. Colloid Interface Sci.*, 2022, **606**, 272–285.
38 X. Wang, Z. Liu, G. Li, G. Jiang, Y. Zhao, L. Li, K. Li, G. Liang, S. Gao, H. Xi, *et al.*, *Chem. Eng. J.*, 2022, **440**, 135764–135776.
39 C. Zhou, C. Zheng, F. Liu, B. Yang, S. Zhang, H. Chen, S. Bai, C. Lin, C.-A. Tao and P. Ye, *Sep. Purif. Technol.*, 2025, **378**, 134516–134521.
40 H. Furukawa, F. Gándara, Y.-B. Zhang, J. Jiang, W. L. Queen, M. R. Hudson and O. M. Yaghi, *J. Am. Chem. Soc.*, 2014, **136**, 4369–4381.
41 I. del Castillo-Velilla, A. Sousaraei, I. Romero-Muñiz, C. S. J. Castillo-Blas, A. Méndez, F. E. Oropeza, V. A. de la Peña O'Shea, J. Cabanillas-González, A. Mavrandonakis and A. E. Platero-Prats, *Nat. Commun.*, 2023, **14**, 2506–2515.
42 Z. Wang, Z. Li, H. Wang, Y. Zhao, Q. Xia, J. Qiu and J. Wang, *ACS Sustainable Chem. Eng.*, 2022, **10**, 10945–10954.
43 C. Zhou, F. Liu, Q. Wu, H. Chen, L. Li, J. Kang, B. Yang and P. Ye, *Chem. Eng. J.*, 2025, 171484.